Wave setup over a Pacific Island fringing reef

O. Vetter,[1] J. M. Becker,[2] M. A. Merrifield,[1] A.-C. Pequignet,[1] J. Aucan,[3] S. J. Boc,[4] and C. E. Pollock[4]

Received 8 June 2010; revised 16 September 2010; accepted 13 October 2010; published 28 December 2010.

[1] Measurements obtained across a shore-attached, fringing reef on the southeast coast of the island of Guam are examined to determine the relationship between incident waves and wave-driven setup during storm and nonstorm conditions. Wave setup on the reef flat correlates well ($r > 0.95$) and scales near the shore as approximately 35% of the incident root mean square wave height in 8 m water depth. Waves generated by tropical storm Man-Yi result in a 1.3 m setup during the peak of the storm. Predictions based on traditional setup theory (steady state, inviscid cross-shore momentum and depth-limited wave breaking) and an idealized model of localized wave breaking at the fore reef are in agreement with the observations. The reef flat setup is used to estimate a similarity parameter at breaking that is in agreement with observations from a steeply sloping sandy beach. A weak (~10%) increase in setup is observed across the reef flat during wave events. The inclusion of bottom stress in the cross-shore momentum balance may account for a portion of this signal, but this assessment is inconclusive as the reef flat currents in some cases are in the wrong direction to account for the increase. An independent check of fringing reef setup dynamics is carried out for measurements at the neighboring island of Saipan with good agreement.

Citation: Vetter, O., J. M. Becker, M. A. Merrifield, A.-C. Pequignet, J. Aucan, S. J. Boc, and C. E. Pollock (2010), Wave setup over a Pacific Island fringing reef, *J. Geophys. Res.*, *115*, C12066, doi:10.1029/2010JC006455.

1. Introduction

[2] During storm events, an important component of elevated sea level at the shoreline is breaking wave setup. Observational studies of wave setup on sandy shorelines have been carried out and the dominant dynamical balances first proposed by *Longuet-Higgins and Stewart* [1962, 1964] confirmed for alongshore uniform bathymetries [e.g., *Guza and Thornton*, 1981; *Lentz and Raubenheimer*, 1999; *Raubenheimer et al.*, 2001]. The dynamical interpretation of observations of wave setup on coral reefs, however, is complicated by differences in reef morphologies and roughness among the study sites and additionally whether the shoreward edge of the reef is bounded by a lagoon or beach [e.g., *Gourlay*, 1996; *Monismith*, 2007].

[3] Early reports of wave setup were made by *Munk and Sargent* [1948] based on visual observations at Bikini Atoll reef. More recent observations of wave setup over coral reefs typically have been made during weak to moderate incident wave conditions. For example, *Gerritsen* [1981] conducted a field experiment at the 200 m wide reef fronting a narrow lagoon at Ala Moana, Oahu, HI and observed maximum setup on the reef of 10.7 cm by differencing the water level from two tide gages. *Lugo-Fernandez et al.* [1998b] measured sea level differences of 4 cm and wave setup of 1 cm across Tague Reef, St. Croix, USVI; however, the interpretation of these setup observations was complicated by inaccuracies in their estimates of the radiation stress. *Lugo-Fernandez et al.* [1998a] observed setup of 0.8–1.5 cm over Great Pond Bay, St Croix, USVI and compared these observations with the model of *Tait* [1972] with reasonable agreement. *Hench et al.* [2008] measuredup to ~25 cm setup at PaoPao Bay, Moorea, French Polynesia, and demonstrated that this setup drives a highly frictional back reef flow. In addition, *Hench et al.* [2008] found that the observed setup varied strongly with significant wave height and period.

[4] The aforementioned observations of setup were made on reefs bounded by lagoons. For a reef bounded by a shoreline, *Jago et al.* [2007] measured a maximum setup of 13.8 cm across a coral reef for incident significant wave heights of 0.4 m. They demonstrated that the tidal elevation on the reef resulted in distinct setup systems with reef edge setup dominant at low tide, shoreline setup dominant at high tide and a dual setup system of reef edge and shoreline setup at midtide.

[5] Observations of setup over coral reefs during storm wave conditions are limited. Inferences have been made

[1]Department of Oceanography, School of Ocean and Earth Science and Technology, University of Hawaii at Manoa, Honolulu, Hawaii, USA.
[2]Department of Geology and Geophysics, School of Ocean and Earth Science and Technology, University of Hawaii at Manoa, Honolulu, Hawaii, USA.
[3]Bermuda Institute of Ocean Sciences, St. Georges's, Bermuda.
[4]Coastal and Hydraulics Laboratory, U.S. Army Engineer Research Center, Vicksburg, Mississippi, USA.

0148-0227/10/2010JC006455

based on *Gourlay* [1996] who used laboratory experiments to estimate the relative wave setup, $\frac{\overline{\eta}_r}{T\sqrt{gH_0}}$, as a function of a submergence parameter, $\frac{\overline{\eta}_r+h_r}{H_0}$, for a variety of two-dimensional reef profiles including both fringing and platform reefs. Here $\overline{\eta}_r$ is the maximum setup, T is the wave period, g is gravity, H_0 is the off reef wave height (rms for irregular waves) and h_r is the water level on the reef in the absence of setup. These experimentally derived relationships [*Gourlay*, 1996, Figure 12] then were applied to predict the magnitude of the wave setup observed during storm conditions at three sites. For example, wave hindcasting estimates of significant wave height and period and tidal estimates during tropical cyclone Ofa (February 1990) allowed the calculation of wave setup ranging from 1.92 to 2.43 m which agree well with the inferred setup of 2.1 m, determined from a newspaper photograph of overflow at the causeway between Lifuka and Foa Islands, Tonga.

[6] The Pacific Island Land Ocean Typhoon experiment (PILOT) sponsored by the U.S. Army Corps of Engineers, was designed to obtain observations of waves and wave-driven flows along reef-fringed island shorelines in an effort to develop and refine predictive models of coastal flooding due to storm waves and typhoons. The main study site is Ipan reef on the southeast coast of Guam, which is composed of a narrow sandy shore connected to a shallow 450 m wide fringing reef flat. Here we assess the magnitude of reef flat setup as a function of measured wave heights for storm and nonstorm conditions.

[7] The PILOT field study provides an opportunity to test setup theory for a fringing reef with high roughness on the fore reef, and low roughness on the reef flat. In addition, we examine whether the dynamics of setup over the reef platform differs from setup observed over sand beach environments. We analyze six weeks of data collected from Ipan Reef in mid-September through October 2009 when incident swell events of 2–3.9 m significant wave height (H_s) occurred, and in July 2007 when tropical storm Man-Yi passed within 200 nm of Guam, causing significant wave heights of 4.6 m in 8 m water depth and 1.3 m peak setup at Ipan. We also consider reef flat observations from deployment E (October–December 2006).

[8] Our findings show that reef flat setup is highly correlated with incident wave height and consistent with the *Longuet-Higgins and Stewart* [1962] setup balance for localized breaking. During moderate wave conditions, setup at Ipan reef is uniform across the width of the reef due to wave breaking localized at the reef edge, with wind wave band energy decaying within 40 m landward of the breakpoint. During large wave events, and particularly during Man-Yi, setup increases shoreward consistent with additional dissipation on the reef flat.

[9] The paper is organized as follows. We begin in section 2 with a description of the study site, the conditions of the experiment and a discussion of wave transformation over the reef. In section 3, we present our observations of wave-driven water level changes and show that the wave setup on the reef flat is highly correlated with incident wave height and scales as approximately 35% of the incident root mean square (*rms*) wave height in ~8 m water depth. In section 4, we revisit the theory of [*Longuet-Higgins and Stewart*, 1962] for a point break and present a simple expression that relates reef flat setup to breaking wave height. The idealized point break model and the reef flat setup observations are used to estimate a similarity parameter at breaking that is similar to that found for steep, sandy beaches [*Raubenheimer et al.*, 1996]. We also consider the effects of bottom stress due to reef flat currents on the cross-shore structure of the setup in section 4. We conclude in section 5 with a discussion of our results.

2. The Study Site

[10] The study site is at Ipan on the southeast coast of Guam. The reef flat is approximately 450 m wide from a narrow sandy shore to the reef crest (~0.3 m deep on average), and is relatively flat and featureless with an average depth of ~0.6 m on the mid-reef flat (Figure 1 and Table 1). The fore reef is steep (4° slope) with irregular and rough topography ranging from individual coral heads to boulders and spur and groove topography. The tides at Guam are mixed semidiurnal/diurnal with a mean range of 0.5 m and a typical spring tide range of 0.7 m. The reef flat typically is exposed during spring low tides. The reef is subject to trade wind waves and occasional tropical storms and typhoons [*Lobban and Schefter*, 1997].

[11] A cross-shore array of bottom-mounted pressure sensors (Seabird SBE26plus) and combined pressure sensors and acoustic velocimeters (Nortek Aquadopp) was deployed across the Ipan reef (Figure 1). Deployments of 3–6 months of varying number of instruments and sampling schemes were carried out from August 2005 to April 2010. The three subsets of data used in this study (Table 1) were collected between mid-September–November 2009 (deployment N), mid-October and mid-December 2006 (deployment E) and during July 2007 (deployment G, or Man-Yi). All data were collected at 1 Hz sample frequency in bursts of varying duration and interval (see Table 1 for sampling details). On the reef face, the current was measured over a 1 m depth cell with a blanking distance of 1 m (i.e., current measurements started 1 m above the bottom). Currents on the reef flat were measured 10 cm above the bottom with varying cell size depending upon location (Table 1). In what follows, we focus on the N and Man-Yi deployments. Due to a timing problem with sensor 8 in deployment E, we only use the reef flat sensors of E in the following analyses.

[12] Mean water levels, $\overline{h}_i$ (i = 1−8), are computed over 15 min intervals and corrected for atmospheric pressure variations using a Seabird deployed on land. Using a pressure threshold, we exclude from our analysis data at times when the reef instruments were not submerged. Estimates of the Bernoulli effect following *Raubenheimer et al.* [2001] are found to have a negligible (<2%) effect on the pressure measurements. The sea surface elevation in the wind wave frequency band (0.04 Hz < f < 0.3 Hz) is estimated from bottom pressure measurements using linear wave theory, significant wave heights H_s are computed as four times the square root of the first moment of the spectrum in this band and the *rms* wave height is $H = 0.706\ H_s$. Changes in water temperature on the reef account for an error of less than 0.2% in the estimation of sea surface elevation from the pressure sensors.

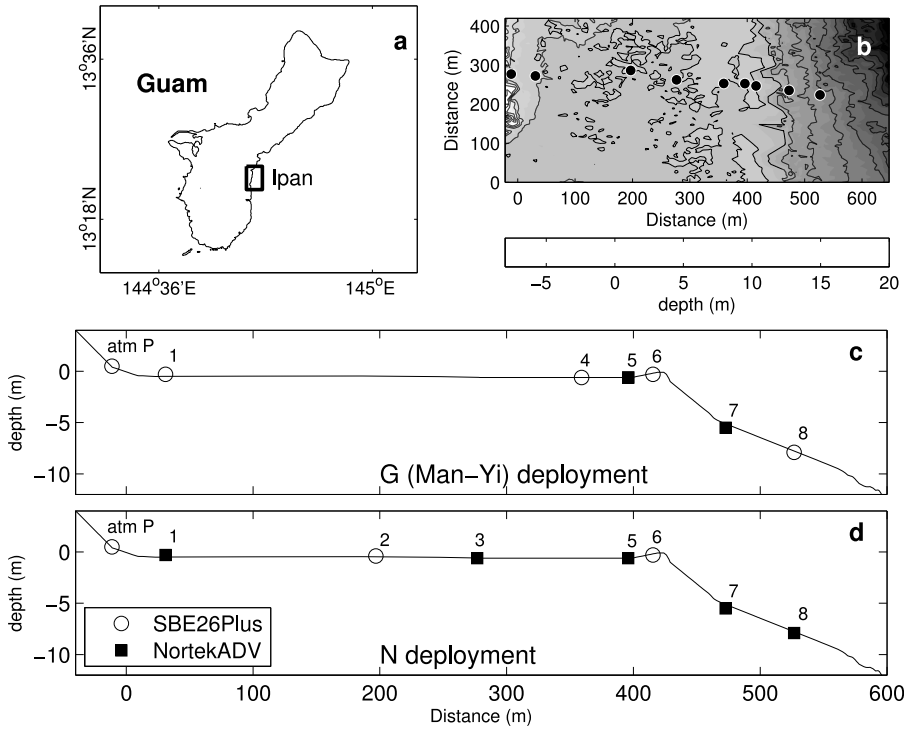

Figure 1. (a) Location of Ipan reef, Guam. (b) Bathymetry of Ipan reef from SHOALS data. Cross-shore bathymetry of Ipan reef from SHOALS data for (c) deployment G and (d) deployment N. Black squares are the locations of collocated pressure and velocimeter sensors (ADVs), and open circles are locations of single pressure sensors at Ipan (SBEs, see Table 1).

[13] Time series of offshore *rms H*, peak period, T_p, and wave direction from North (Figure 2) were obtained from a Datawell directional wave buoy operated by the Coastal Data Information Program (CDIP) of the Scripps Institution of Oceanography located offshore in 200 m of water approximately 2.4 km from the reef array. The two deployment periods include several moderate wave events during winter conditions (deployment N) and a large wave event generated by tropical storm Man-Yi during summer conditions (deployment G). The winter events (Figure 2, left) range in wave height and peak period from 2 to 4 m and from 8 to 16 s while the *rms* wave height at the CDIP buoy during Man-Yi reached 5 m with a peak period of approximately 11 s.

[14] In the following analysis, we reference wave setup on the reef flat to the conditions at our most offshore instrument $i = 8$ in 8 m water depth. We choose H_8 as the reference wave height as significant attenuation occurs between the measured wave height at the offshore buoy and our sensor 8 during events arriving from the south. The difference between buoy and 8 m wave heights are particularly significant during the peak of tropical storm Man-Yi. Wave transformation from the CDIP buoy to the reef face will be examined in a future study.

[15] As discussed by A.-C. Pequignet et al. (Sea and swell wave energy on the reef-fringed shoreline of Ipan, Guam, submitted to *Coral Reefs*, 2010), incident wind wave energy at Ipan is strongly attenuated at the reef crest and over the outer reef flat due to wave breaking (Figure 3, see also *Massel and Gourlay* [2000]). Starting at the fore reef, we find that the *rms* wave heights in ~6 m and ~8 m water depth (H_7 and H_8) are similar, except for the largest wave events, in particular during the peak of Man-Yi (Figure 3a, right). For moderate wave heights, the energy flux on the reef face between 8 and 7 is approximately conserved. For the largest wave events, the wave heights observed at sensor 7 are smaller than those predicted by conservation of energy flux consistent with dissipation (either wave breaking or bottom stress) or nonlinear transfer of energy out of the wind wave band occurring on the fore reef. We note that an estimate of the effects of refraction between sensors 8 and 7 is too small to account for the observed decrease in wave height. Wave breaking reduces significantly the wave height measured on the shoreward side of the reef crest (Figure 3b), between sensors 7 and 6. Wave heights at sensor 7 in 6 m water depth and sensor 6 on the reef crest are correlated ($r = 0.87$ over both deployments) with a regression coefficient of $b = 0.26$. Further decay in wave height across the reef flat to the shore (Figure 3c) is presumably due to bottom friction or, during the largest wave events, additional breaking on the reef flat (Pequignet et al., submitted manuscript, 2010). We also note that on the reef flat (e.g., sensor 3), *rms* wave heights in the wind wave band depend upon water level. Increased breaking and frictional effects at low tide result in smaller reef flat wave heights H_3 for a fixed incident wave height H_8 (Figure 4).

[16] The steep, irregular nature of the fore reef topography at Ipan did not allow us to obtain pressure measurements near where breaking typically occurs (between sensors 7 and 6). On the reef flat, the extent to which waves are depth limited is examined with a linear regression of H_i and water

Table 1. Instrument Sampling Schemes for Deployments N, E, and G With Approximate Mean Sensor Depth Specified With Sensor Number[a]

Sensor	Position	N (Sep–Nov 2009)	E (Oct–Dec 2006)	G (Jul 2007)
1 (0.3 m)	30 m	PUV: 10,800 s every 4 h (0.2:0.1 m)	P: 2048 s every 3 h	P: 43180 s every 12 h
2 (0.4 m)	195 m	P: 43,180 s every 12 h		
3 (0.6 m)	277 m	PUV: 10,800 s every 4 h (0.2:0.1 m)		
4 (0.6 m)	359 m		PUV: 2048 s every 3 h (0.2:0.1 m)	P: 43,180 s every 12 h
5 (0.6 m)	396 m	PUV: 10,800 s every 4 h (0.2:0.1 m)	P: 2048 every 3 h	PUV: 7200 s every 4 h (0.3:0.1 m)
6 (0.3 m)	416 m	P: 43,180 s every 12 h	PUV: 2048 s every 3 h (0.1:0.1 m)	P: 43,180 s every 12 h
7 (5.6 m)	475 m	PUV: 10,800 every 4 h (1:1 m)	PUV: 2048 s every 3 h (1:1 m)	PUV: 7200 s every 4 h (1:1 m)
8 (7.9 m)	530 m	PUV: 10,800 every 4 h (1:1 m)	P: 2048 s every 3 h	P: 43,180 s every 12 h

[a]Position is distance from the shore. P indicates a pressure measurement (Seabird pressure sensor, SBE), while PUV indicates a pressure-current measurement (Nortek Aquadopp, ADV). Velocities from the Aquadopps are specified with (cell size: blanking distances).

depth, $\overline{h}_i$, at the reef flat sensors with SBEs (i = 1, 4, 6) yielding the similarity parameter, γ_i

$$H_i = \gamma_i \overline{h}_i. \quad (1)$$

We limit our regression to water depths greater than 0.3 m ($\overline{h}_i > 0.3$ m) and find that γ_i varies across the reef (Figure 5). On the reef flat, waves are weaker for a given water level at the inner-reef sensor (γ_1 = 0.13 ± 0.02) compared to the

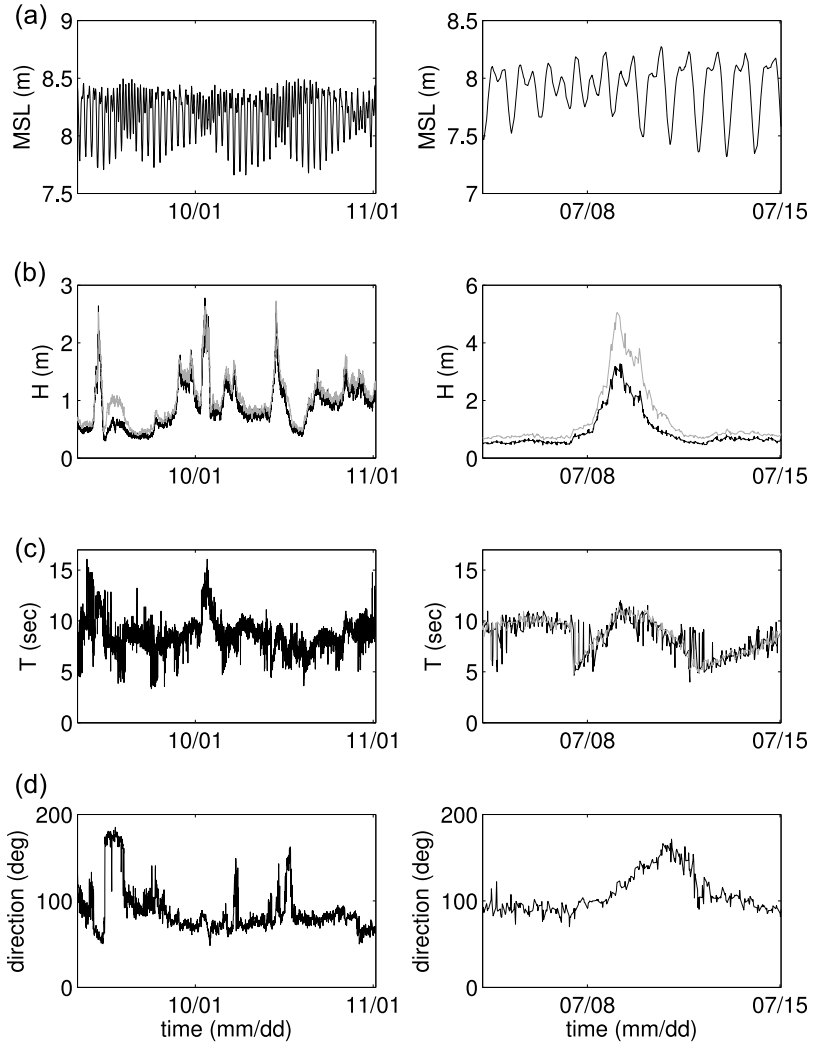

Figure 2. Conditions during deployments N and G at Ipan. (left) The conditions during the winter of deployment N (September to November 2009). (right) The conditions during Man-Yi during deployment G (July 2007). (a) The sea level at the most offshore instrument location (sensor 8 in ~8 m water depth). (b and c) The *rms* wave height and peak period from sensor 8 (black line) and the CDIP buoy (gray line). (d) The wave direction from north from the CDIP buoy.

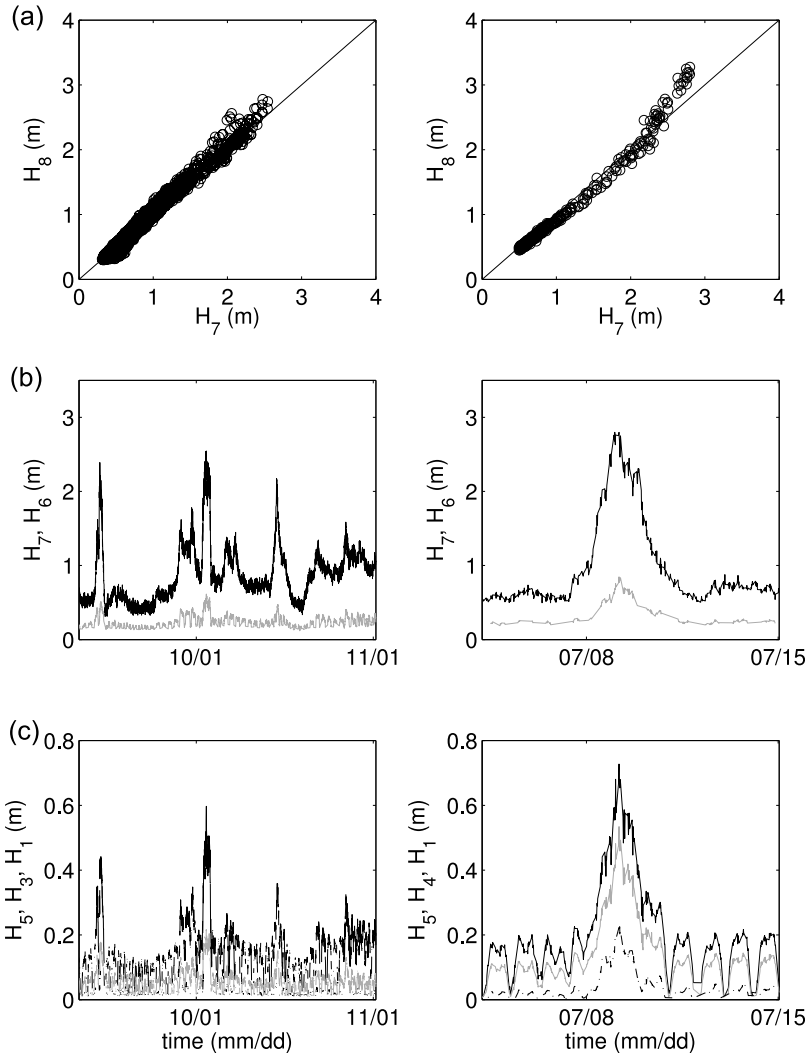

Figure 3. The *rms* wave height H_i during the (left) winter deployment (N) and (right) ManYi (G). (a) The relationship between reef face wave heights H_8 versus H_7. (b) Time series of the reef face sensor H_7 (black line) and the most seaward reef flat sensor H_6 (gray line) where breaking has reduced the wave heights significantly. (c) Time series of reef flat wave heights H_5 (black line), H_3 (gray line), H_1 (black dash-dotted line) for N and H_5 (black line), H_4 (gray line), H_1 (black dash-dotted line) for ManYi.

mid-reef ($\gamma_4 = 0.22 \pm 0.01$). The reef crest has $\gamma_6 = 0.96 \pm 0.04$, which may be due to wave shoaling and breaking at the shallow reef edge. The error bars quoted are the 95% confidence limits assuming data separated by 8 h are independent. On the mid to inner reef, the decrease in γ_i toward shore is presumably due to waves breaking at the shallow reef crest (i.e., the reef crest is shallower than the local depth at locations $i = 1$–5), and to the effect of friction in the wave bottom boundary layer [*Lowe et al.*, 2005], which leads to wave dissipation above a depth-limited breaking condition.

[17] As mentioned above, we were unable to obtain observational estimates of γ on the steep reef face where breaking occurs. In what follows, we estimate a γ_b associated with depth limited breaking from our setup observations presented in section 3 and the setup dynamics of *Longuet-Higgins and Stewart* [1962] for localized wave breaking (section 4.1) and show this estimate to be consistent with that measured for a steeply sloping sand beach [*Raubenheimer et al.*, 1996].

3. Setup Observations

[18] We calculate the observed setup η_i from the 15 min averages of water level, $\overline{h}_i$. Setup results obtained using 30 min average water levels are similar; hence, the 15 min averaging is sufficient to filter the infragravity signal from these estimates. We reference our setup estimates to sensor 8. During deployment N, the mean water level at sensor 8 is approximately 0.3 m higher than during deployments E and Man-Yi which we suspect is due to a displacement of the instrument or a calibration offset error rather than a change in sea level. This offset, however, does not affect our estimates of setup or breaking wave height below. We assume that the setdown at sensor 8, η_8, is negligible (but see below)

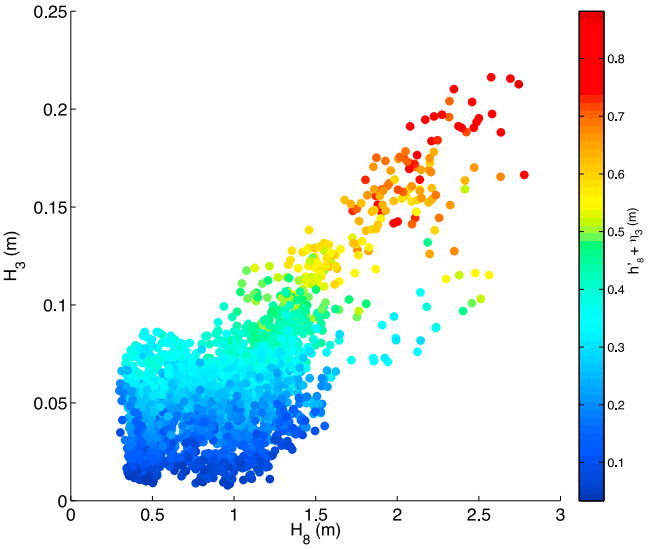

Figure 4. Water level effects on reef flat wave height. Reef flat *rms* wave height H_3 versus incident wave height H_8, with color indicating the water depth at sensor 8 with the mean removed h_8', plus the setup at sensor 3. Wave heights where $\overline{h}_3 < 0.3$ m are excluded.

and set $\eta_8 \equiv 0$, hence the mean water level to which the setup estimates are referenced is $\overline{h}_8$.

[19] We obtain the wave-driven change in water level at sensors 1 through 7 by differencing $\overline{h}_8$ and $\overline{h}_i$

$$\mathrm{d}\overline{h}_i = \overline{h}_i - \overline{h}_8 \tag{2}$$

and then performing a regression of the form

$$\mathrm{d}\overline{h}_i = aH_8 + bt + c \tag{3}$$

where H_8 is the 8 m observed wave height and t is time. The regression is used to account for drifts over time, which is an issue for pressure transducers, and to select a reference offset, c, so that setup is zero when $H_8 = 0$. At sensor 7, where water level is set-down as the waves shoal on the fore reef, we replace H_8 with H_8^2 in (3) to match the theoretical relationship between setdown and offshore wave height [*Longuet-Higgins and Stewart*, 1962] and (5) below.

[20] The wave-driven change in water level at sensor i then is estimated as

$$\eta_i = \mathrm{d}\overline{h}_i - bt - c, \qquad (i = 1 - 7). \tag{4}$$

The observed setdown in 6 m water depth, η_7, is noisy and during Man-Yi, larger than the predicted setdown from [*Longuet-Higgins and Stewart*, 1962]

$$\tilde{\eta} = -\frac{H^2 k}{8 \sinh 2kh}, \tag{5}$$

(correlation $r = 0.88$ for Man-Yi, $r = 0.59$ for N, Figure 6). As a second estimate of the observed setup, we assume that setdown occurs in 8 m water depth at sensor 8 and is approximated by (5). The mean water level to which the setup estimates are referenced then is taken as the water level at 8 less the estimated setdown at 8, $h_0 = \overline{h}_8 - \tilde{\eta}_8$. The η_i, $i = 1$–7 then are estimated following the procedure above with h_0 replacing $\overline{h}_8$ in (2). As $\tilde{\eta}_8$ predicted from (5) is smaller than $\tilde{\eta}_7$ (Figure 6), we find that the shoreline setup estimates referenced to h_0 do not differ significantly (~7%) from those referenced to $\overline{h}_8$. In what follows, we present observed setup estimates from (2) to (4) referenced to $\overline{h}_8$.

[21] Scatterplots of the setup η_i computed from (2) to (4) versus incident wave height H_8 for the winter deployment (Figure 7, top, N), and during Man-Yi (Figure 8, top, G) reveal that setup increases significantly between sensor 6 at the reef crest and sensor 5 just shoreward of the reef crest and then is relatively constant on the reef flat except during the peak of Man-Yi when setup is observed to increase shoreward. For all reef flat sensors (1–6), setup is well correlated ($r_i > 0.95$) with the 8 m wave height H_8. Regression coefficients, b_{i8}, between setup at sensor i and H_8 and (95% confidence intervals are approximately 0.01 for all sensors) are given by $b_{18} = 0.39$, $b_{48} = 0.38$, $b_{58} = 0.37$, and $b_{68} = 0.30$ for deployment Man-Yi. For deployment N, we find $b_{18} = 0.32$, $b_{28} = 0.33$, $b_{38} = 0.32$, $b_{58} = 0.30$ and $b_{68} = 0.21$.

[22] For deployment N (Figure 7, bottom), we present time series of setup/down estimates at $i = 7$, 6, 2 for clarity as the setup estimates η_i, $i = 1$, 3 are similar to $i = 2$. The large setup on the reef flat observed during Man-Yi increases toward shore (sensors 6–1), with significant set down occuring at sensor 7 during the peak of the storm (Figure 8, bottom). Gaps in the observed setup estimates occur when the reef top sensors are exposed.

4. Setup Theory

4.1. Setup: Wave Breaking on the Reef Face

[23] Assuming no alongshore variation in waves or bathymetry and negligible surface and bottom stresses, *Longuet-Higgins and Stewart* [1962] showed that the

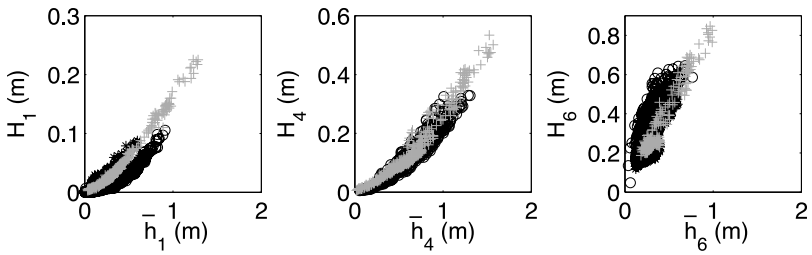

Figure 5. The *rms* wave height H_i versus water depth $\overline{h}_i$ for reef flat SBE sensors $i = 1$, 4, 6 for N (black asterisk), E (black circle), and ManYi (gray plus sign).

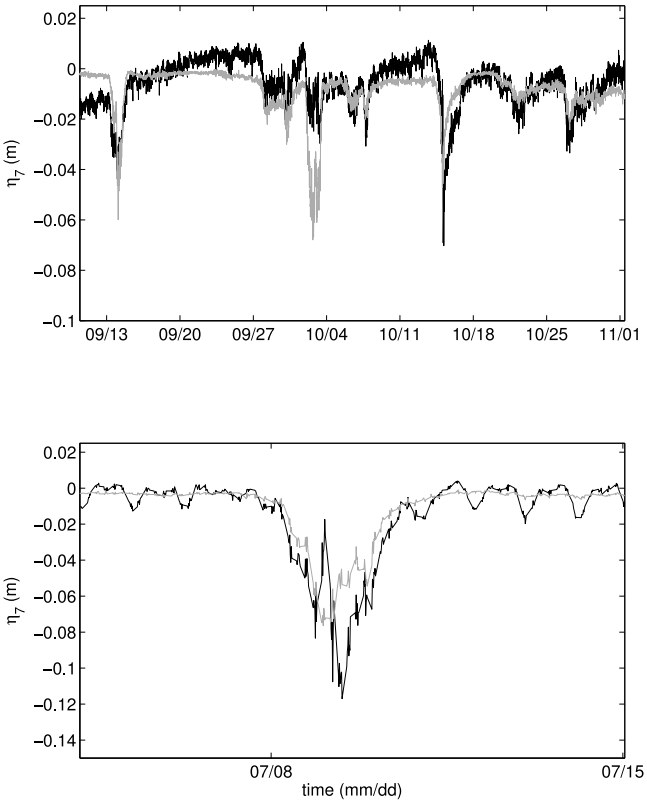

Figure 6. Observed setdown η_7 estimated from sensor 2 to 4 (black line) and from *Longuet-Higgins and Stewart* [1962] (equation (5)) (gray line) for deployments (top) N and (bottom) ManYi.

horizontal momentum balance that governs the wave setup, $\tilde{\eta}$, is given by

$$\frac{dS_{xx}}{dx} + \rho g(\tilde{\eta} + h)\frac{d\tilde{\eta}}{dx} = 0, \tag{6}$$

where S_{xx} is the radiation stress, and h is the mean water level in the absence of waves. We note that the observed 15 min average water depth, $\overline{h} = \tilde{\eta} + h$, includes the setup. Previous studies [e.g., *Guza and Thornton*, 1981; *King et al.*, 1990; *Lentz and Raubenheimer*, 1999; *Raubenheimer et al.*, 2001], have tested (6) against water level observations with good success. The most detailed comparison to date invokes realistic wave transformation models and includes bottom stress due to undertow in the balance (6) [*Apotsos et al.*, 2007].

[24] Due to the localized nature of wave breaking on the steep reef face at Ipan, we demonstrate that a simple analytic expression similar to *Battjes* [1974] reproduces the reef flat setup for the majority of wave conditions observed. We consider the dynamics (6) for an idealized model of wave breaking at a point where

$$H(x) = (H_r - H_{8b}(x))\mathcal{H}(x - x_b) + H_{8b}(x) \qquad x_8 < x < x_r \tag{7}$$

and $\mathcal{H}$ is the Heaviside step function. In (7), $H_{8b}(x)$ represents the wave height between sensor 8 (8 m water depth) and the breakpoint at x_b and ranges from H_8 at $x = x_8$ to the estimated value of the wave height at breaking H_b at x_b (see (17)). This model is chosen based on visual observations of a single breakpoint on the steep fore reef for a range of incident wave conditions [*Hilmer*, 2005]. In this simplified model, the residual wave height is H_r at position x_r after breaking. We next assume that breaking occurs in shallow water where the radiation stress is given by

$$S_{xx} = \frac{3}{2}E \tag{8}$$

where

$$E = \frac{1}{8}\rho g H^2 \tag{9}$$

is the wave energy. In addition, we take the breaking wave height to be depth limited according to

$$H_b = \gamma_b(\tilde{\eta}_b + h_b) \equiv \gamma_b \overline{h}_b \tag{10}$$

where γ_b is a similarity parameter.

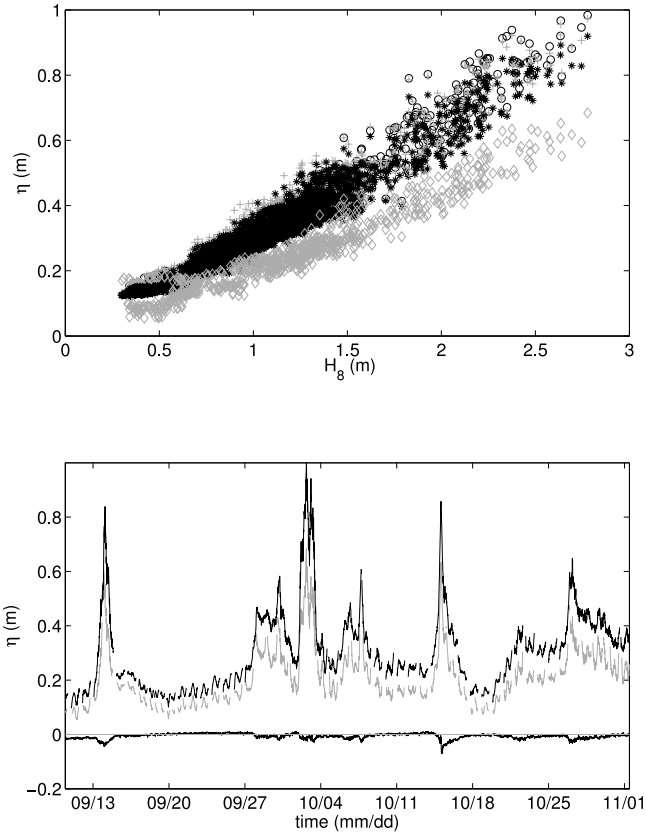

Figure 7. Setup across the reef for N. (top) The observed reef flat setup η versus incident wave height H_8. The reef flat setup increases from near the reef crest shoreward and is indicated by gray diamond (sensor 6), black asterisk (sensor 5), gray plus sign (sensor 3), and black circle (sensor 1). (bottom) A time series of setup/setdown referenced to zero setdown at 8 (gray horizontal line) with setdown at sensor 7 (black line), setup at sensor 6 (gray line), and setup at sensor 2 (black line).

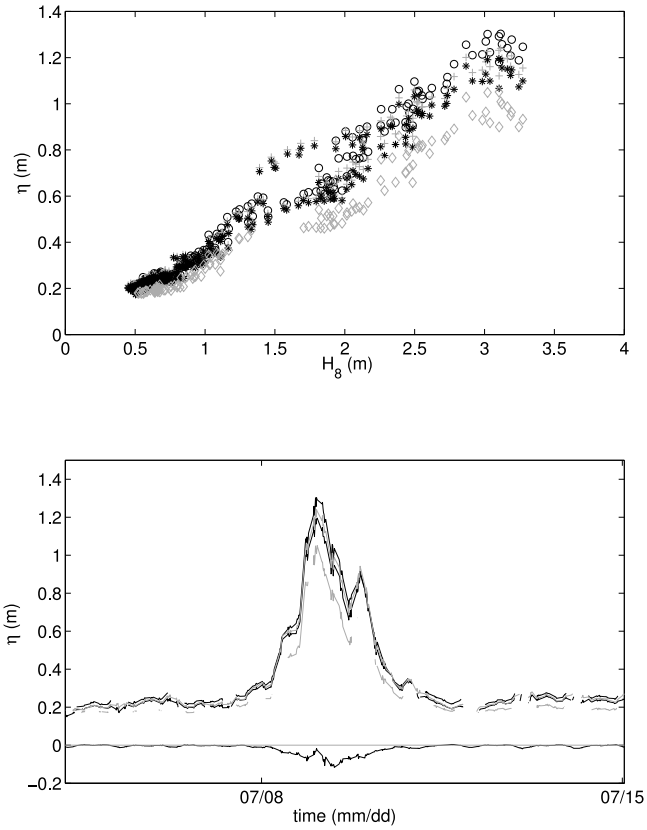

Figure 8. Setup across the reef for ManYi. (top) The observed reef flat setup η versus incident wave height H_8. The reef flat setup increases from near the reef crest shoreward and is indicated by gray diamond (sensor 6), black asterisk (sensor 5), gray plus sign (sensor 4), and black circle (sensor 1). (bottom) A time series of setup/setdown referenced to zero setdown at sensor 8 (gray horizontal line) at all instruments with alternating gray and black lines.

[25] It is straightforward to show that (6), (8) and (9) may be combined to yield

$$\frac{\mathrm{d}\eta}{\mathrm{d}x} = -\frac{3H}{8(\tilde{\eta}+h)}\frac{\mathrm{d}H}{\mathrm{d}x}. \tag{11}$$

Evaluating $\frac{\mathrm{d}H}{\mathrm{d}x}$ using our simple transformation model (7) we obtain

$$\frac{\mathrm{d}H}{\mathrm{d}x} = (H_r - H_{8b})\delta(x - x_b) + (1 - \mathcal{H}(x - x_b))\frac{\mathrm{d}H_{8b}(x)}{\mathrm{d}x} \tag{12}$$

where $\delta(x)$ is the Dirac delta function. Substituting (12) in (11), integrating from the breakpoint, x_b, to a point shoreward of the breakpoint, x_r, and invoking (10), we obtain

$$\tilde{\eta}_r - \tilde{\eta}_b = \frac{3}{8}\gamma_b(H_b - H_r) \tag{13}$$

where $\tilde{\eta}_b$ is the setdown at the breakpoint. We note that (13) is independent of the form of $H_{8b}(x)$, the wave height seaward of the breakpoint. Moreover, while the similarity parameter defining depth limited wave heights, γ, depends upon position (Figure 5), γ_b is that value of γ evaluated at $x = x_b$.

[26] We substitute (10) into the shallow water limit of (5) and approximate the setdown at the breakpoint as

$$\tilde{\eta}_b \approx -\frac{1}{16}\gamma_b H_b. \tag{14}$$

Invoking (14), (13) becomes

$$\tilde{\eta}_r = \frac{5}{16}\gamma_b H_b - \frac{3}{8}\gamma_b H_r. \tag{15}$$

At the shore, we assume $H_r \ll H_b$, and (15) becomes

$$\tilde{\eta}_1 = \frac{5}{16}\gamma_b H_b \tag{16}$$

which is equivalent to the expression derived by *Battjes* [1974] (his equation 3.4.8), assuming constant similarity parameter γ.

[27] We next use our setup observations at sensor 5 on the reef flat, η_5, (15) and an estimate of the breaking wave height H_b to obtain an estimate of the similarity parameter at breaking, γ_b. We chose sensor 5 as representative of reef flat setup as it is shoreward of the region of active breaking near the reef crest (i.e., sensor 6), but has not been affected significantly by dissipation on the reef flat. We estimate the breaking wave height H_b by assuming conservation of energy flux between sensor 8 and the breakpoint and depth limited breaking, (10), and obtain

$$\overline{h}_b = \left(\frac{8\mathcal{F}_8}{\rho g^{3/2}\gamma_b^2}\right)^{2/5}, \qquad H_b = \gamma_b \overline{h}_b \tag{17}$$

where $\mathcal{F}_8$ is the energy flux integrated over frequency at sensor 8. Given the estimated depth at the breakpoint and the observed peak periods, we use the shallow water approximation at the breakpoint in (17).

[28] To determine γ_b, we use an initial guess of γ_b in (17) to obtain an initial estimate of H_b. The observed η_5 then is regressed on the estimated H_b following (15) with the residual wave height term treated as an intercept to obtain a second estimate of γ_b. This procedure converges within a few iterations to an estimate of γ_b that is consistent with the observed η_5 and estimated H_b.

[29] We find $\gamma_b = 0.91 \pm 0.03$ for deployment N where the estimated breaking water depth, h_b ranges from ~2–3 m during wave events (Figure 9a), and $\gamma_b = 1.13 \pm 0.09$ for ManYi with $h_b \approx 3$ m (Figure 9b). The higher value of γ_b for the ManYi deployment over the N deployment may be due to differences in the location of the breakpoint on the steep reef face as estimates of γ for sandy beaches have been shown to be slope dependent [*Raubenheimer et al.*, 1996], or to additional dynamical contributions to setup that are not included in the idealized point break model (see section 4.2 below). Additionally, as expected, using these values of γ_b in (16) provides an excellent estimate of setup at the shoreline η_1 over the range of wave heights observed (not shown).

[30] We note that the predicted breakpoint occurs between instruments $i = 7$ and 6, which is consistent with observations for moderate wave heights, and suggests that breaking

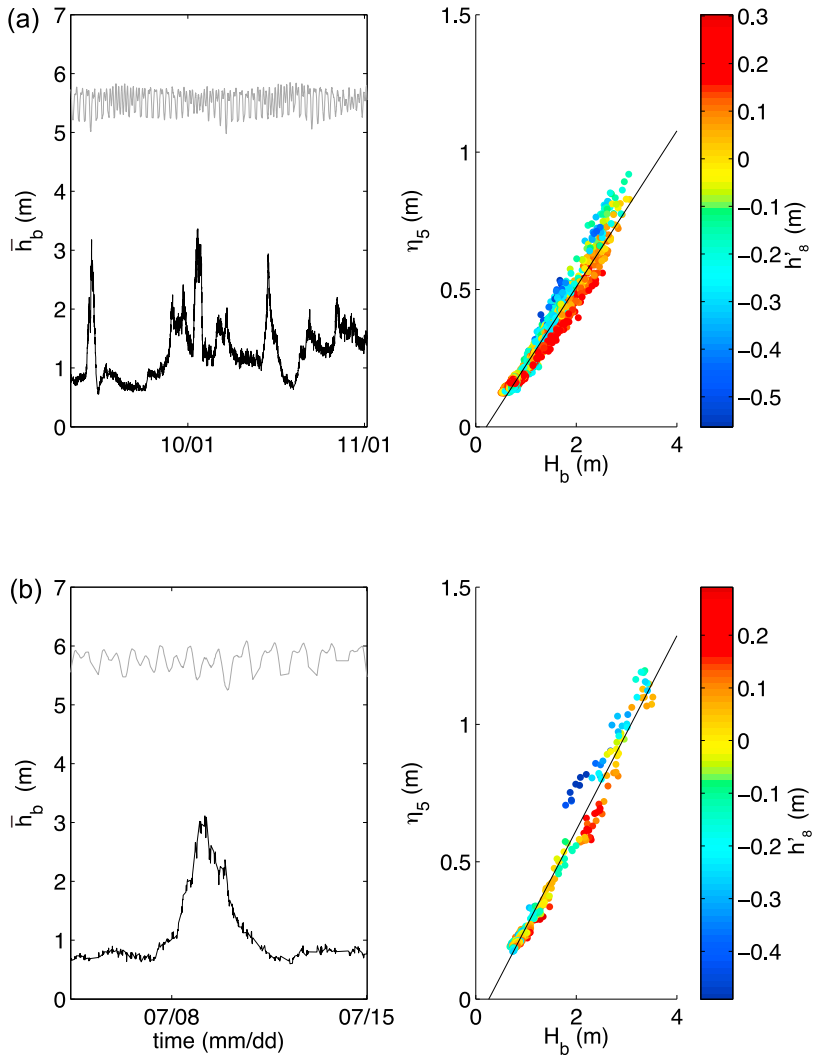

Figure 9. (left) Estimated water depth at breaking $\overline{h}_b$ (black line) and (right) observed reef flat setup η_5 versus estimated breaking wave height H_b for deployments (a) N and (b) Man-Yi. The color bar indicates the water depth at sensor 8 with the mean removed, and the black line is the regression between η_5 and H_b. The water depth at breaking $\overline{h}_b$ and breaking wave height H_b are estimated from (15), (17), and the observed η_5, H_8, and $\overline{h}_8$. Also shown is water level at sensor 7 for both deployments (Figure 9, left, gray trace). Data for which $\overline{h}_5 < 0.3$ m are excluded from the scatterplots.

may not be responsible for the decrease in wave height observed between sensors 8 and 7 during the peak of ManYi (Figure 3, section 2). We also remark that for a given incident wave height, more setup is observed on the reef flat at low tide than at high tide (Figure 9, right), consistent with increased breaking at low tide (Figure 4).

[31] The values obtained for γ_b above are derived for *rms* wave height and when referenced to significant wave height are approximately 40% larger. *Raubenheimer et al.* [1996, Figure 8c] found values of γ referenced to significant wave height ranging from approximately 0.4 to 1.3 for a steeply sloping sandy beach (slope = 0.0825). The γ_b values derived here for Ipan (reef face slope $\approx$ 0.07) lie at the upper end of this range.

[32] The single breakpoint model used here does not account for the sharp increase in setup between the reef crest η_6 and the next shoreward sensor 20 m from the crest η_5. We consider sensor 6 to be in a shallow zone of active breaking adjacent to the steep reef face. Our observations are not sufficient to resolve the detailed physics of this narrow zone. We do note, however, that the estimated radiation stress gradients between sensors 6 and 5 are too small to account for the observed increase in setup.

4.2. Setup: Bottom Stress on the Reef Flat

[33] We next consider the cross-shore structure of the reef flat setup. For deployment N, as mentioned above, we find that the setup increases significantly between sensors 6 and 5 and then increases slightly across the reef flat between sensors 5 and 2. During the Man-Yi deployment, the observed setup increases shoreward at all reef flat sensors (Figure 8).

[34] Here we demonstrate that the cross-shore increase in setup on the reef flat between sensors 4 and 1 may be due to

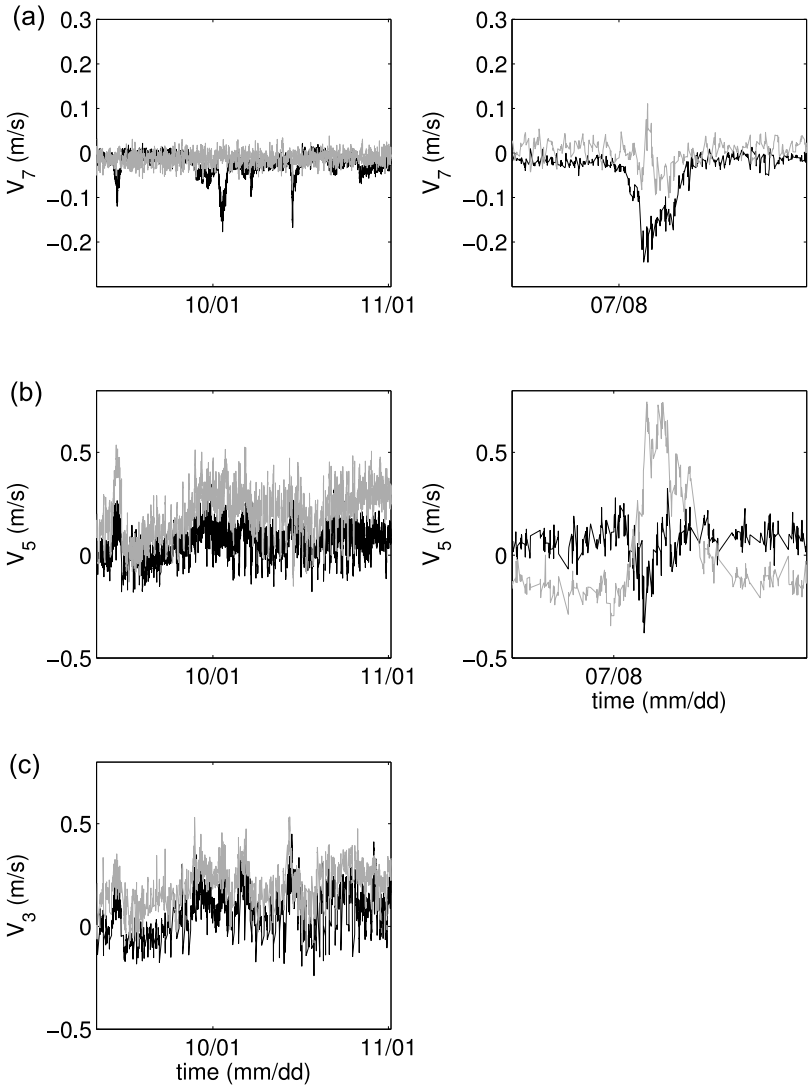

Figure 10. Average cross-shore (u, black) and alongshore (v, gray) currents for deployments (left) N and (right) Man-Yi. Positive currents directed onshore/southward. (a) The 15 min average reef-face currents at sensor 7. (b and c) The 15 min average of reef flat currents as sensors 5 and 3 (N only). Data for $\overline{h}_5 <$ 0.4 m and $\overline{h}_3 < 0.4$ m during deployment N and $\overline{h}_5 < 0.5$ m during Man-Yi are excluded.

the effects of bottom stress during Man-Yi when offshore currents were observed; however, it appears that bottom stress is not responsible for the increase in setup shoreward during deployment N when onshore reef flat currents were observed. As mentioned above, the inclusion of bottom stress in the dynamics, (6), following [*Longuet-Higgins*, 2005], has been shown to increase shoreline setup for sandy beaches with undertow [*Apotsos et al.*, 2007].

[35] Cross-shore (positive onshore) and alongshore (positive southward) currents, (u, v), were measured on the reef face and reef flat during both deployments (Figure 10 and Table 1). Fifteen minute averages of reef flat currents measured approximately 0.2 m above the bottom (i.e., measured over a 0.2 m cell, 0.1 m above the bottom) are onshore during deployment N at sensors 3 and 5. For the Man-Yi deployment, during low wave conditions, average cross-shore reef flat currents measured approximately 0.3 m above the bottom at sensor 5 also are onshore, while offshore currents are observed at sensor 5 on the reef flat during the peak of Man-Yi. We do not have measurements of the vertical structure of the current; however, during sensor deployments and recoveries, the flow on the reef flat was unidirectional with depth with no indication of an undertow. Alongshore currents on the reef flat are southward during the winter deployment N, and during the Man-Yi event. The average cross-shore currents approximately 1.5 m above the bottom on the reef face (sensor 7, Figure 10) are offshore during both deployments and are highly correlated with incident wave height ($r = -0.9$). The alongshore flows on the reef face are smaller than those observed on the reef flat, with the largest alongshore currents observed during Man-Yi.

[36] We estimate cross-shore bottom stress, τ_{bc}, from the measured currents on the reef flat according to

$$\tau_{bc} = \rho C \langle |\mathbf{u}| u \rangle \tag{18}$$

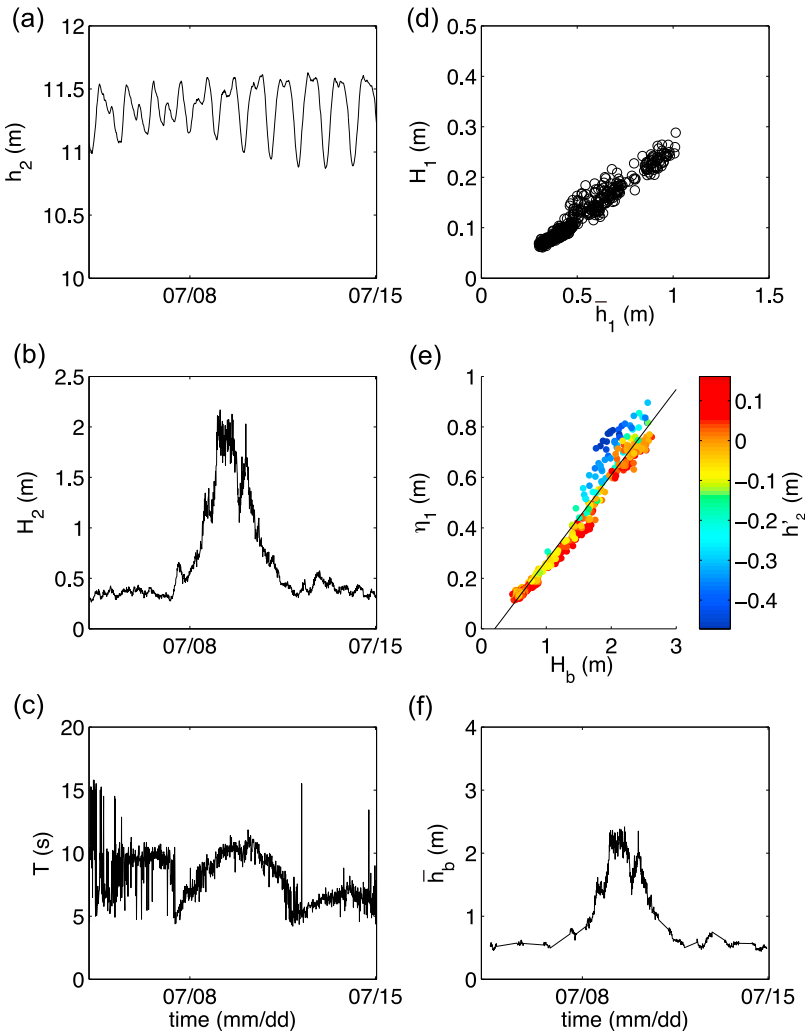

Figure 11. Reef face conditions (Figures 11a–11c) and reef flat setup (Figure 11e) at Laulau Bay, Saipan. Reef face: (a) water depth h_2, (b) *rms* wave height H_2, and (c) period T_2. Reef flat: (d) *rms* wave height H_1 versus water depth $\overline{h}_1$; (e) observed setup η_1 versus breaking wave height H_b; and (f) estimated water depth at breaking $\overline{h}_b$. The color bar indicates the water depth at 2 with the mean removed h_2', and the black line is the regression between η_1 and H_b.

where C is a friction coefficient and $\langle \cdot \rangle$ denotes a 15 min time average. In (18), $\mathbf{u} = (u, v)$ is the (cross-shore, alongshore) current just outside the bottom boundary layer. We do not have a direct estimate of the boundary layer structure over the reef flat; however, for this approximation, we take $\mathbf{u}$ as the measured current in 0.2/0.3 m depth for deployment N/Man-Yi.

[37] We estimate the bottom stress necessary to explain the increase in reef flat setup, τ_b, from our observations during Man-Yi and the horizontal momentum balance (6) with bottom stress [*Longuet-Higgins*, 2005]

$$\tau_b = -\frac{\mathrm{d}S_{xx}}{\mathrm{d}x} - \rho g(\overline{\eta} + h)\frac{\mathrm{d}\overline{\eta}}{\mathrm{d}x}. \qquad (19)$$

We evaluate the right-hand side of (19) from the observed setup, *rms* wave heights and water depths using a forward difference approximation to the radiation stress gradient and setup slope between sensors 4 and 1 on the reef flat to obtain an estimate of the bottom stress between sensors 4 and 1, $\tau_b = \tau_{41}$. We consider conditions when incident wave heights are greater than 1 m and water levels are greater than 0.3 m over the Seabirds and 0.5 m over the Aquadopp. We remark that τ_{41} is an estimate of the average bottom stress between sensors 4 and 1 while τ_{bc} is estimated at sensor 5. Observations of the velocities at sensors 5 and 3 during deployment N demonstrate that currents are relatively uniform on the reef flat, hence, the point estimate of τ_{bc} at sensor 5 is a reasonable estimate of reef flat bottom stress between sensors 4 and 1.

[38] While the data are too noisy to estimate the drag coefficient C from a regression of $\langle |\mathbf{u}|u \rangle$ on τ_{41}, (19), we find that for a drag coefficient of $C \sim 0.006$, the two estimates of bottom stress are in reasonable agreement during the peak of Man-Yi. We note that the value of C used here is smaller than that estimated by *Apotsos et al.* [2007] (0.018–0.028), but similar to previous drag coefficient estimates for alongshore currents (e.g., 0.002–0.003, *Feddersen et al.*

[1998], 0.001–0.012 *Garcez-Faria et al.* [1998], see also additional estimates quoted by *Apotsos et al.* [2007]). We find, however, that for the majority of our observations, reef flat currents are onshore and in the wrong direction for bottom stress to account for the shoreward increase in reef flat setup observed during the wave events of deployment N. Onshore currents have been linked to a decrease in setup across reef flats by *Gourlay and Colleter* [2005]; however, such a decrease is not evident in our observations. While cross-shore currents may account for the shoreward increase in reef flat setup during Man-Yi, we note that the storm affected local winds, with sustained winds peaking near 15 m/s and wind directions shifting from northerly to southerly over the course of the event. Storm wind-forcing also might account for an increase in water levels at the coast.

4.3. Laulau Bay, Saipan

[39] As an independent check of the dynamics of section 4.1, we repeat the analysis of section 3 above for observations from a deployment at Laulau Bay, Saipan (15°09′38″N, 145°45′11″E). The reef characteristics are similar to Ipan, but the reef flat is shorter (~135 m). Two Seabird pressure sensors were deployed on the fore reef and reef flat of Laulau Bay during the G deployment and sampled for 43,180 s every 12 h at 1 Hz. The conditions at the reef face sensor SBE2 (approximately 143 m offshore of the reef edge in 11.3 m water depth) are presented in Figures 11a–11c. The conditions at the reef flat sensor SBE1 (approximately mid-reef flat in 0.4 m water depth) are presented in Figures 11d–11f. The water depth on the reef flat, $\overline{h}_1$, is highly correlated (r = 0.98) with *rms* wave height H_1 (Figure 11d), with a regression coefficient of b = 0.24 similar to the mid-reef regression coefficients at Ipan (Figure 5). For consistency with the Ipan data, we approximate the wave height in 8 m water depth at Saipan $H8$ using conservation of energy flux from the reef face sensor SBE2. The observed setup (computed from (2)–(4) for i = 1, 2) referenced to $H8$ is highly correlated (r = 0.98) with 8 m wave height and the regression coefficient between $H8$ and η_1 of 0.38 ± 0.01 is similar to the mid reef values for Ipan (not shown).

[40] We also estimate the depth limited similarity parameter at breaking, γ_b, breaking wave height H_b and water depth at breaking h_b iteratively from (15), (17) η_1 and the 8 m wave height H8. We find for the Saipan data that γ_b = 1.09 ± 0.09 (Figure 11e) similar to that obtained for Ipan during tropical storm Man-Yi. We also remark that, similar to Ipan (Figure 4), for the same incident wave heights, larger values of setup are observed at low tide than at high tide, consistent with increased breaking at low tide (Figure 4).

5. Summary and Discussion

[41] Field observations have been collected from a fringing reef at Ipan, Guam with no back lagoon separating the reef crest from the shoreline. Previous observational studies of wave setup over fringing reefs [*Jago et al.*, 2007] typically have been limited to weak wave conditions. Here we present observations of setup for incident significant wave heights that exceed 4 m during tropical storm Man-Yi. Wave breaking at the reef face and crest lead to the setup of the reef flat, with the setup highly correlated with (r = 0.95) and scaling as approximately 35% of the *rms* wave height in ~8 m depth.

[42] The steady, inviscid cross-shore momentum dynamics of *Longuet-Higgins and Stewart* [1962] for an idealized point break wave transformation model and depth-limited breaking are consistent with the high correlation observed between incident wave height and reef flat setup. The Ipan observations suggest a depth-limited breaking parameter of γ_b ~ 0.9–1.1, which is shown to agree with independent observations collected at the nearby island of Saipan, and with observations of wave breaking on a steep sandy beach [*Raubenheimer et al.*, 1996]. Extending the cross-shore momentum balance to include bottom stress modeled from measured currents is shown to be consistent with the observed increase (~10%) in setup shoreward during tropical storm Man-Yi, when reef flat currents were offshore, but not during the wave events of deployment N when reef flat currents were onshore.

[43] The results presented here appear to be applicable to shore-attached fringing reefs with shallow depths over the reef flat and a steep fore reef, which favor a limited breaking zone that is well modeled by equation (7). Friction appears to have a limited effect on the cross-shelf mean momentum balance. We note that the Ipan reef flat is fairly smooth and featureless- the influence of friction may be considerably higher over a rough platform. The details of wave transformation over the fore reef and reef crest require further study. While our estimate of wave breaker depth oversimplifies the actual transformation process over the rough, steep terrain, our approach nevertheless provides useful estimates of reef flat setup amplitudes given incident wave amplitudes at the fore reef.

[44] **Acknowledgments.** C. Kontoes, T. Hilmer, K. Millikan, and Y. Firing assisted with the Ipan field experiment. We also thank the staff at the University of Guam Marine Laboratory for their help during our field deployments and in particular Jason Miller for his invaluable contribution to the diving operation. J. Gove and colleagues at the Coral Reef Ecosystem Division of the NOAA National Marine Fisheries Service deployed and recovered sensors at Saipan. The wave buoy data were provided by the Coastal Data Information Program (CDIP) at the University of California, San Diego (UCSD). The project was funded by the U.S. Army Corps of Engineers via a subcontract through UCSD. Project support provided by J. Thomas (UCSD) and R. Jensen and A. Garcia (USACE) is greatly appreciated. This paper is funded in part (ACP) by a grant/cooperative agreement from the National Oceanic and Atmospheric Administration, Project R/EP-31, which is sponsored by the University of Hawaii Sea Grant College Program, SOEST, under Institutional grant NA05OAR4171048 from NOAA Office of Sea Grant, Department of Commerce. The views expressed herein are those of the authors and do not necessarily reflect the views of NOAA or any of its subagencies. UNIHI-SEAGRANT-JC-07-19.

References

Apotsos, A., B. Raubenheimer, S. Elgar, R. T. Guza, and J. A. Smith (2007), Effects of wave rollers and bottom stress on wave setup, *J. Geophys. Res.*, *112*, C02003, doi:10.1029/2006JC003549.

Battjes, J. A. (1974), Computation of setup, longshore currents, runup and overtopping due to wind-generated waves, *Rep. 74-2*, Delft Univ. of Technol., Delft, Netherlands.

Feddersen, F., R. T. Guza, S. Elgar, and T. H. C. Herbers (1998), Alongshore momentum balances in the nearshore, *J. Geophys. Res.*, *103*(C8), 15,667–15,676, doi:10.1029/98JC01270.

Garcez-Faria, A. F., E. B. Thornton, T. P. Stanton, C. V. Soares, and T. C. Lippmann (1998), Vertical profiles of longshore currents and related bed shear stress and bottom roughness, *J. Geophys. Res.*, *103* (C2), 3217–3232, doi:10.1029/97JC02265.

Gerritsen, F. (1981), Wave attenuation and wave setup on a coastal reef, *Tech. Rep. 48*, Look Lab., Univ. of Hawaii at Manoa, Honolulu.

Gourlay, M. R. (1996), Wave setup on coral reefs. Part 2. Set-up on reefs with various profiles, *Coastal Eng.*, *28*, 17–55.

Gourlay, M. R., and G. Colleter (2005), Wave-generated flow on coral reefs: An analysis for two-dimensional horizontal reef-tops with steep faces, *Coastal Eng.*, *52*, 353–387.

Guza, R. T., and E. B. Thornton (1981), Wave setup on a natural beach, *J. Geophys. Res.*, *86*(C5), 4133–4137, doi:10.1029/JC086iC05p04133.

Hench, J. L., J. J. Leichter, and S. G. Monismith (2008), Episodic circulation and exchange in a wave-driven coral reef and lagoon system, *Limnol. Oceanogr.*, *53*, 2681–2694.

Hilmer, T. (2005), Measuring breaking wave heights using video, G.E.S. senior thesis, Sch. of Ocean and Earth Sci. and Technol., Univ. of Hawaii at Manoa, Honolulu.

Jago, O. K., P. S. Kench, and R. W. Brander (2007), Field observations of wave-driven water-level gradients across a coral reef flat, *J. Geophys. Res.*, *112*, C06027, doi:10.1029/2006JC003740.

King, B. A., M. W. L. Blackely, A. P. Carr, and P. J. Hardcastle (1990), Observations of wave-induced setup on a natural beach, *J. Geophys. Res.*, *95*(C12), 22,289–22,297, doi:10.1029/JC095iC12p22289.

Lentz, S., and B. Raubenheimer (1999), Field observations of wave setup, *J. Geophys. Res.*, *104*(C11), 25,867–25,875, doi:10.1029/1999JC900239.

Lobban, C. S., and M. Schefter (1997), *Tropical Pacific Island Environments*, Univ. of Guam Press, Mangilao, Guam.

Longuet-Higgins, M. S. (2005), On wave setup in shoaling water with a rough seabed, *J. Fluid Mech.*, *527*, 217–234.

Longuet-Higgins, M. S., and R. W. Stewart (1962), Radiation stress and mass transport in gravity waves, with application to "surf-beats," *J. Fluid Mech.*, *13*, 481–504.

Longuet-Higgins, M. S., and R. W. Stewart (1964), Radiation stresses in water waves: A physical discussion with application, *Deep Sea Res. Oceanogr. Abstr.*, *11*, 529–562.

Lowe, R. J., J. L. Falter, M. D. Bandet, G. Pawlak, M. J. Atkinson, S. G. Monismith, and J. R. Koseff (2005), Spectral wave dissipation over a barrier reef, *J. Geophys. Res.*, *110*, C04001, doi:10.1029/2004JC002711.

Lugo-Fernandez, A., H. H. Roberts, and J. N. Suhayda (1998a), Wave transformations across a Caribbean fringing-barrier coral reef, *Cont. Shelf Res.*, *18*, 1099–1124.

Lugo-Fernandez, A., H. H. Roberts, and W. J. Wiseman (1998b), Tide effects on wave attenuation and wave setup on a Caribbean coral reef, *Estuarine Coastal Shelf Sci.*, *47*, 385–393.

Massel, S. R., and M. R. Gourlay (2000), On the modelling of wave breaking and setup on coral reefs, *Coastal Eng.*, *39*, 1–27.

Monismith, S. G. (2007), Hydrodynamics of coral reefs, *Annu. Rev. Fluid Mech.*, *39*, 37–55.

Munk, W. H., and M. C. Sargent (1948), Adjustment of Bikini Atoll to ocean waves, *EOS Trans. AGU*, *29*, 855–860.

Raubenheimer, B., R. T. Guza, and S. Elgar (1996), Wave transformation across the inner surf zone, *J. Geophys. Res.*, *101*(C11), 25,589–25,597, doi:10.1029/96JC02433.

Raubenheimer, B., R. T. Guza, and S. Elgar (2001), Field observations of wave-driven setdown and setup, *J. Geophys. Res.*, *106*(C3), 4629–4638, doi:10.1029/2000JC000572.

Tait, R. J. (1972), Wave setup on coral reefs, *J. Geophys. Res.*, *77*(12), 2207–2211, doi:10.1029/JC077i012p02207.

J. Aucan, Bermuda Institute of Ocean Sciences, 17 Biological Station, Ferry Reach, St. Georges's GE 01, Bermuda.

J. M. Becker, Department of Geology and Geophysics, School of Ocean and Earth Science and Technology, University of Hawaii at Manoa, POST Building, Suite 701, 1680 East-West Rd., Honolulu, HI 96822, USA. (jbecker@soest.hawaii.edu)

S. J. Boc and C. E. Pollock, Coastal and Hydraulics Laboratory, U.S. Army Engineer Research Center, 3909 Halls Ferry Rd., Vicksburg, MS 39180, USA.

M. A. Merrifield, A.-C. Pequignet, and O. Vetter, Department of Oceanography, School of Ocean and Earth Science and Technology, University of Hawaii at Manoa, Marine Science Building, Suite 205, 1000 Pope Rd., Honolulu, HI 96822, USA.